Experimental Demonstration of Error Recovery in an Integrated Cyberphysical Digital-Microfluidic Platform*

Kai Hu, Mohamed Ibrahim, Liji Chen, Zipeng Li, Krishnendu Chakrabarty, and Richard Fair

***Abstract*—Digital (droplet-based) microfluidics enables the integration of fluid-handling operations and reaction-outcome detection. Despite these benefits, defects and erroneous fluidic operations continue to be major barriers to the adoption and deployment of these devices. We describe the first practical and fully integrated cyberphysical error-recovery system that can be implemented in real time on a field-programmable gate array (FPGA). The hardware-assisted solution is based on an error dictionary containing the error-recovery plans for various anticipated errors. The dictionary is computed and stored in FPGA memory before the start of the biochemical experiment. Errors in droplet operations on the digital microfluidic platform are detected using capacitive sensors, the test outcome is interpreted by control hardware, and corresponding error-recovery plans are triggered in real-time. Experimental results are reported for a fabricated silicon device, and links to videos are provided for the first-ever experimental demonstration of real-time error recovery in cyberphysical digital-microfluidic biochips using a hardware-implemented dictionary.**

I. Introduction

Chip-scale adaptation of biochemical applications using digital microfluidics technology is now becoming increasingly popular [1], [2]. Several studies have recently been reported for empowering digital-microfluidic biochips (DMFBs) with a control system that can enable real-time recovery from errors during bioassay execution [3]–[6]. These errors might occur due to a variety of reasons, e.g., physical defects, charge trapping because of excessive electrode actuation [7], or protein fouling [8], and they may lead to malfunctions in specific parts of the biochip [8].

Among these studies, the work in [4] was the first to present an experimental demonstration of error recovery in cyberphysical DMFBs. However, in this study, Hu et al. used a software approach to accomplish dynamic reconfiguration for the biochip. In order to generate the new electrode actuation sequences for recovery, a desktop computer is involved in the control system. The drawbacks of this approach are: (1) increased complexity of the cyberphysical system; (2) then need for a software-resynthesis step, which leads to increased bioassay response time when errors occur.

The computer-in-the-loop control approach has also been used in [9]; a real-time electrode-driving technique was proposed to manipulate multiple-droplets. The DMFB system in [9] achieves fault tolerance by using a fuzzy-enhanced control system that is able to identify deteriorated electrodes and flexibly adjust droplet routes in real-time. However, the complex inference engine significantly increases the overall system complexity and leads to timing overhead. In [10], the electrode-driving technique was enhanced to increase droplet velocities while elongating the lifetime of the biochip. The control system in [10] also involves a desktop computer that controls biochip actuation through an FPGA board according to the feedback from a high-speed camera system.

Instead of using a software-based solution, we have implemented dictionary-based hardware-assisted error recovery. For a target set of errors that can occur in a bioassay, simulations are used to generate an error dictionary before the experiments are conducted. During simulation, erroneous fluidic operations are considered and the corresponding error recovery plans are determined and then stored as entries in the dictionary. Once an error is detected during the experiment, the control system triggers the corresponding error-recovery plan based on the error dictionary.

The dictionary-based error recovery can be implemented using a finite-state machine (FSM). The control signals for the biochip are determined by the current state of the FSM; an integrated sensor is used to provide the feedback that indicates whether an error has occurred. If an error is detected, a state transition in the FSM is triggered. The error dictionary stored in the FPGA memory is a precomputed database that links each possible state to the corresponding control signals for the biochip. The dictionary is stored as a decision tree, where each branch/entry records all possible errors and their corresponding error-recovery plans. When the sensing system detects an error, the FSM transitions to the corresponding faulty state and the linked entry in the error dictionary is loaded and sent to the chip for error recovery.

In this paper, we describe the first integrated demonstration of cyberphysical digital microfluidics, where errors in droplet transportation on the biochip array are detected using capacitive sensors. The interpretation of the test outcome and the decision-making process are accomplished using a hardware system. Experimental results are reported based on a fabricated silicon device and links to videos [11] are provided to highlight the capability of hardware-based real-time control of multiple droplets, autonomous error detection through capacitance sensing, and the human-intervention-free re-routing of droplets to bypass faulty sites.

*This work was supported in part by the National Science Foundation under grant CNS-1135853. The authors are with the department of Electrical and Computer Engineering, Duke University, Durham, NC 27708, USA.

978-1-4799-7234-0/15/$31.00 ©2015 IEEE

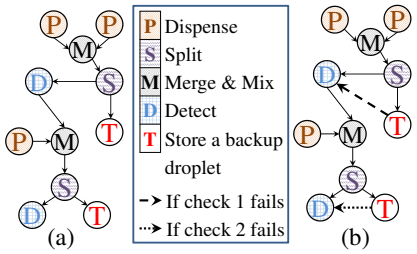

Fig. 1: Sequencing graph for dilution: (a) Fault-free execution; (b) Utilization of on-chip backup droplets for error recovery.

II. Experiment Design

In this section, we describe the experiment design and validation plan to demonstrate the proposed dictionary-based cyberphysical error-recovery system.

A. Protocol Design and Error Recovery

Our system has been designed to autonomously execute typical assay protocols empowered with the capacity to perform error recovery. In this paper, a typical dilution protocol is used to exemplify the utilization of our control system.

The executed dilution protocol aims at using a set of reagents to dilute an input sample into a targeted mixture/concentration. The description of the executed protocol is given by the sequencing graph in Fig. 1(a). The vertices represent the bioassay operations, whereas the edges represent the interdependencies among these operations. As shown in the figure, the protocol requires dispensing three droplets (i.e., "P" operation) for execution. After each split "S" operation, one droplet is considered as a backup droplet and is routed into one of the chip boundaries to be stored, whereas the other droplet is driven into the detector cell. This cell is linked to a capacitance measurement circuit used to test for droplet presence/absence status. A typical biochip can be equipped with several sensor circuits to form multiple checkpoints, however increasing the number of checkpoints increases the cost of the system hardware. Therefore, we monitor the dilution protocol droplets in our chip using only one checkpoint.

When the sensor circuit reports a "missing droplet", we infer that a fault exists on the path used for driving the droplet.

Fig. 1(b) shows how the dilution protocol sequence is updated so that recovery actions are considered in missing-droplet cases. After each split, if the to-be-detected droplet is reported to be missing, the control system loads recovery actuation sequences from the hardware memory. In this action, the stored backup droplet is used as replacement for recovering from this error and continuing the operations. If no backup droplet exists, a new droplet has to be dispensed from the reservoir and the sequence must be repeated.

B. Biochip Layout and Checkpoint Localization

Our experimental chip (fabrication details are discussed in Section IV), whose layout is shown in Fig. 2, consists of 32 electrodes that are independently controlled by external pins. The cell in blue shows the location of the checkpoint. Based on the pre-computed actuation sequences, we know the clock cycles when the droplets are expected to reach the detector cell. If a droplet is reported to be missing, a recovery action is invoked in the manner that was explained in the previous subsection.

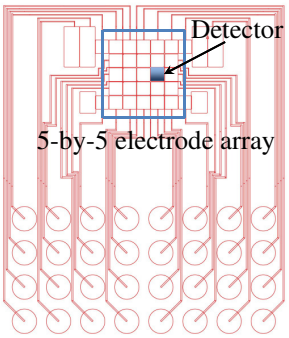

Fig. 2: The layout of the fabricated biochip.

C. Back-end Algorithmic Support for the Control System

The error recovery system depends solely on the hardware for generating recovery actuation sequences whenever an error is detected. The dictionary-based approach, however, requires a back-end software support that is capable of extracting protocol specification from the user (including covered errors), modeling the dictionary components to generate the recovery sequences, and feeding the hardware controller with the required scripts and files for bioassay execution and error recovery. The inputs to the software tool are: (1) the protocol description which can be provided by the user or extracted from a droplet routing CAD tool. (2) The pin mapping file which is used to map the electrodes to the actuating FPGA pins. The output is a memory file whose values are stored in the FPGA memory.

In order to incorporate error recovery in our control system, the software tool must be aware of all possible recovery scenarios that need to be included. This information can either be driven directly by the user or as a result to an offline synthesis by a high-level synthesis tool [12]. Hence, the back-end software models the underlying hardware finite-state machine by flattening it into a decision tree. To illustrate this concept, suppose that it is required to provide the control information needed to execute the dilution protocol, shown in Fig. 1(b), while considering recovery from a potential error detected during check #1. In this case, the control information for both error-free as well as erroneous execution are communicated to the back-end software tool to build a decision tree (we call it execution tree). Note that this tree is translated later to a finite-state machine in the hardware.

Having identified the nodes of the execution tree via the input file, the back-end software tool is capable of generating the memory file and logging the start addresses of every node represented in the tree. These addresses are used by the hardware control system during its state transitions in order to adapt the system to the sensor readouts.

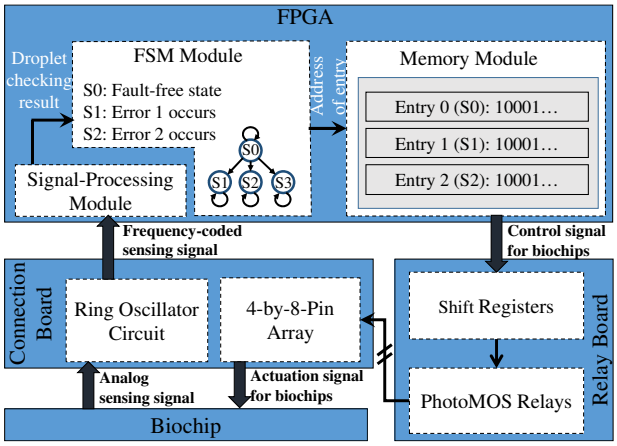

Fig. 3: Schematic of the integrated system setup.

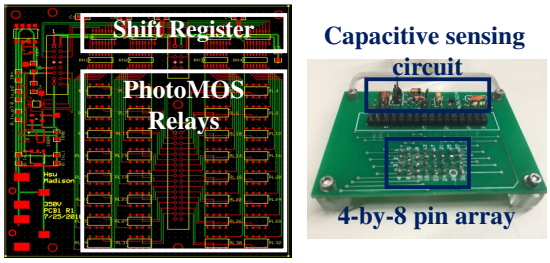

(a) (b)

Fig. 4: The actuation system: (a) The layout of the relay board; (b) Image of the connection board.

III. Implementation of Error Recovery

The integrated system consists of three parts: a relay board, a connection board, and an FPGA with integrated memory. Fig. 3 shows a schematic of the integrated system setup.

A. Relay Board

The relay board, whose image is shown in Fig. 4(a), is used to synchronously actuate the 32 electrodes in the biochip. The input to the relay board is the low-voltage control signal provided by the FPGA (0-5 V), and the output is the high-voltage actuation voltage for the biochips (40 V, 1 kHZ AC voltage). Four 8-bit serial-in-parallel-out shift registers (Part No.: 74HC595) and 32 photoMOS relays (Part No.: AQW610S) are integrated on the relay board. The shift registers are used to realize serial-to-parallel conversion of the control signal, and the photoMOS relays are used to convert the signal from the low-voltage control signal to the high-voltage actuation signal for the biochip.

B. Connection Card and Capacitive Sensing Circuit

The connection board, whose image is shown in Fig. 4(b), contains two modules: a 4-by-8-pin array and a ring oscillator circuit used for capacitive sensing. The pin array on the back of the connection board can contact the metal pads on the biochip so that the high-voltage actuation signal is transferred from the relay board to the chip. The circuit diagram for the capacitive sensing can be found in [4] (Fig. 2(a)). The ring oscillator circuit is used to detect the presence or absence of droplets by monitoring the capacitance change between the control and ground electrodes. When a droplet of ionic liquid is present between the electrodes, the majority of the applied electric field forms over the dielectric layer of the biochip. This decreases the charge separation distance in the device and thus increases the capacitance for the overall structure, which lowers the detected output frequency of the ring oscillator circuit. Conversely, if a droplet is absent, the electric field is established over both the dielectric layer and the filler medium (e.g., silicon oil or air). This increases the distance over which charge is separated in the device, thereby decreasing the capacitance measured for the overall structure.

C. FPGA

The circuitry for cyberphysical error recovery consists of three main modules: (1) the signal-processing module that analyzes the frequency feedback signal from the capacitive sensing circuit and determines if an error has occurred, (2) the memory module that stores the error dictionary, and (3) the FSM module that dynamically adjusts the actuation sequences when an error is reported. Fig. 3 illustrates the interconnection between these modules.

1. *Signal-processing module:* The signal-processing module is essentially a frequency counter. It is used to: (1) process the frequency signal collected from the ring oscillator circuit on the connection board, and (2) determine whether an error occurs in the bioassay and report the sensing results to the FSM module. However, an important design challenge arises due to the fact that a 1 kHz AC power source is directly connected to the biocell for the actuation. This AC power source is in close proximity to the capacitance sensor, which leads to significant interference with the capacitance sensing output, which is a frequency-encoded square wave. To reduce this interference, an exact 1 s window is set in the frequency counter to accumulate frequency signals in 1000 periods of the AC source before updating the output.
2. *Memory module:* The memory module is used to store the error dictionary of the bioassay. During the fault simulation of the bioassay, entries of the error dictionary are generated. Note that each entry in the dictionary contains only the resynthesis result from the time that the error is detected to the end of the bioassay. The error dictionary is then written into a memory initialization file (MIF). The MIF specifies the content for each memory cell in the read-only memory (ROM) of the FPGA. The starting and ending addresses of each dictionary entry are simultaneously generated and loaded into the FSM module.
3. *FSM module:* The FSM is used to implement automatic error recovery. The sensing results from the signal-processing module are sent as the input to the FSM, and the outputs from the FSM are the starting and ending storage addresses of the dictionary entry that should be applied to the biochip. When the signal-processing module sends a signal indicating that an error has occurred, the FSM transitions to the corresponding faulty state for error recovery and the starting and ending storage addresses of the dictionary entry are updated accordingly.

When the FSM sends the addresses of the dictionary entry, the data that are stored in the corresponding memory cells are sent to the output of the ROM.

IV. Experiment Results and Demonstration

In this section, we present biochip fabrication details, experimental results, and a demonstration of error recovery.

A. Biochip Fabrication and Chip Specifications

The DMFB device used in the experiment consists of three major components. The gasket is sandwiched between the top plate and the bottom plate to create the operation area for the electrowetting-on-dielectric (EWOD) function. The acrylic top plate is laser cut into the appropriate shape and the pipette holes are also laser cut into the top plate. A layer of ITO is then applied on top of the acrylic to provide the ground plane when the EWOD function is active. The ITO layer is sputtered onto the acrylic plate and its thickness is controlled to be 140 nm. The surface of the top plate needs to be hydrophobic in order for the EWOD function to work. Therefore, CYTOP is spun onto ITO layer of thickness 80 nm. The bottom plate is fabricated based on a silicon substrate of 500 μm thick. On top of the silicon substrate, there is a thin layer of thermal oxide of thickness 1 μm. The electrode is patterned out of the Cr layer. The Cr layer is deposited using EBPVD technique and the thickness of that layer is 100 nm. The electrode is patterned using lithography, resulting in a total of 32 electrodes and connection wires to the contacting pads. Above the Cr layer, the dielectric layer is deposited using Parylene C with thickness of 1.1 μm. The surface is also kept hydrophobic by being spun on a layer of CYTOP of thickness 80 nm.

The device is completed by bonding the top plate and the bottom plate using the gasket layer. The gasket layer is made out of a 120 μm thick adhesive SecureSeal. The SecureSeal is laser cut to define the operation area. The three components is aligned and bonded together after the gasket is ready. Over night vacuum desiccation is used to evaporate the solvent used during the fabrication.

The size of electrode used in the experiment is 1mm $\times$ 1mm. Actuation signals of electrodes are transferred through the contact between the contact pads on the biochip and the pin array on the connection board. The channel height is determined by the gasket thickness, which is 120 μm in our experiment. The volume of the droplet can be hence calculated to be 120 nL. The liquid in the droplet is DI water. During the experiment, the device is filled with 2 cS silicone oil first to prevent the water droplet form evaporation.

B. Results and Videos

The FPGA device used in the experiment was an Altera Cyclone IV with 6.3 Mb embedded memory. The synthesis results show that the signal-processing modules, memory modules, and FSM modules on the FPGA consume a total of 597 logic elements (2% of the available elements), 180 Kb (3% of the available memory) and 10 user I/Os (3% of the available pins). The demo setup is shown in Fig. 5. Several

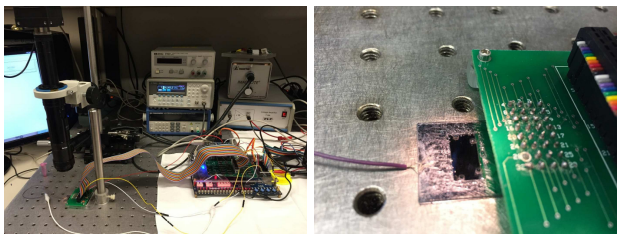

Fig. 5: The experimental setup in the laboratory.

experimental runs were carried out using the fabricated chip and the control system. A CCD camera was used to capture the video, and images were extracted from the recorded video. Videos of the error-recovery experiments are available online [11]. Droplets were routed as discussed in Section II. The fault-free video shows the initial droplet route. If an error occurs, the droplets cannot reach the checkpoints as planned in the experiment. At that point, the corresponding entry in the error dictionary is activated and the error-recovery solution is triggered.

V. Conclusion

We have demonstrated error detection and recovery in a cyberphysical digital-microfluidic biochip. Detection of errors was performed using a capacitive sensor, the test outcome was interpreted by a hardware signal processing module, and error recovery was accomplished through a hardware dictionary.

References

[1] Illumina. (2015) Illumina NeoPrep Library Prep System. [Online]. Available: http://www.illumina.com/systems/neoprep-library-system.html/

[2] H.-H. Shen, S.-K. Fan, C.-J. Kim, and D.-J. Yao, "EWOD microfluidic systems for biomedical applications," *Microfluidics and Nanofluidics*, vol. 16, no. 5, pp. 965–987, 2014.

[3] Y. Luo, K. Chakrabarty, and T.-Y. Ho, "Error recovery in cyberphysical digital microfluidic biochips," *IEEE Trans. Comput.-Aided Design Integr. Circuits Syst.*, vol. 32, no. 1, pp. 59–72, Jan 2013.

[4] K. Hu *et al.*, "Fault detection, real-time error recovery, and experimental demonstration for digital microfluidic biochips," in *Proc. IEEE/ACM Design, Autom., Test Eur. (DATE)*, 2013, pp. 559–564.

[5] Y. Luo, K. Chakrabarty, and T.-Y. Ho, "Real-time error recovery in cyberphysical digital-microfluidic biochips using a compact dictionary," *IEEE Trans. Comput.-Aided Design Integr. Circuits Syst.*, vol. 32, no. 12, pp. 1839–1852, Dec 2013.

[6] M. Alistar, P. Pop, and J. Madsen, "Redundancy optimization for error recovery in digital microfluidic biochips," *Design Automation for Embedded Systems*, pp. 1–31, 2015. [Online]. Available: http://link.springer.com/article/10.1007/s10617-014-9157-2

[7] H. Verheijen and M. Prins, "Reversible electrowetting and trapping of charge: model and experiments," *Langmuir*, vol. 15, no. 20, pp. 6616–6620, 1999.

[8] V. Srinivasan *et al.*, "Protein stamping for MALDI mass spectrometry using an electrowetting-based microfluidic platform," in *Optics East*, 2004, pp. 26–32.

[9] J. Gao *et al.*, "An intelligent digital microfluidic system with fuzzy-enhanced feedback for multi-droplet manipulation," *Lab Chip*, vol. 13, pp. 443–451, 2013.

[10] C. Dong *et al.*, "On the droplet velocity and electrode lifetime of digital microfluidics: voltage actuation techniques and comparison," *Microfluidics and Nanofluidics*, vol. 18, no. 4, pp. 673–683, 2015.

[11] [Online]. Available: http://microfluidics.ee.duke.edu/BioCAS2015_IntegratedErrorRecovery/

[12] T. Xu, K. Chakrabarty, and F. Su, "Defect-aware high-level synthesis and module placement for microfluidic biochips," *IEEE Trans. Biomed. Circuits Syst*, vol. 2, no. 1, pp. 50–62, 2008.